Ocean Engineering 232 (2021) 109125

Contents lists available at ScienceDirect

Ocean Engineering

journal homepage: www.elsevier.com/locate/oceaneng

Short communication

Estimation of multipath delay-Doppler parameters from moving LFM signals in shallow water

Quan Sun [a,b], Fei-Yun Wu [a,b,*], Kunde Yang [a,b], Yuanliang Ma [a,b]

[a] School of Marine Science and Technology, Northwestern Polytechnical University, Xi'an, 710072, China
[b] Key Laboratory of Ocean Acoustics and Sensing, Ministry of Industry and Information Technology, Northwestern Polytechnical University, Xi'an, 710072, China

ARTICLE INFO

Keywords:
Multipath propagation
Delay-doppler estimation
Sparse representation

ABSTRACT

The conventional methods including cross-ambiguity function (CAF) and least square (LS) methods have intensively studied for the estimation of the delay-Doppler parameters from moving linear frequency modulated (LFM) signals. Due to the characteristic of underwater acoustic multipath propagation in shallow water and the mobility of sound source, the traditional methods provide limited resolutions for the lack of sparsity exploitation. This study aims to jointly estimate the multipath delay-Doppler parameters based on a sparse representation model, which leads to a large scale and computational complexity of the dictionary matrix in delay-Doppler framework. To solve the above problems, we propose an orthonormal operation via the Gram-Schmidt method for the delay-Doppler solution during the matching pursuit iterations. The obvious advantage of the proposed approach is to avoid inverse matrix computation, which improves the robustness and effectiveness for the estimation of the delay-Doppler parameters. The simulation and experimental results indicate that the proposed method outperforms the traditional CAF and LS methods both in terms of resolution and accuracy. Furthermore, the proposed method, compared with the ROMP and CoSaMP methods, provides superior performance in terms of mean square error (MSE).

1. Introduction

The multipath acoustic propagation is a common phenomenon in shallow water environments, which usually attracts a lot of attention in the fields of underwater acoustic communication, sonar detection, source localization, and geoacoustic inversion (Cao et al., 2018; Jesus et al., 2000; Mandic et al., 2020; Song et al., 2018). The source-medium-receiver configuration is not steady due to the motion of source or receiver, strong sea currents, and fluctuant boundaries in practical applications. The Doppler effect is commonly used for radial velocity estimation of the moving targets (Liang et al., 2019). Due to the Doppler effect and multipath propagation, the received signal is the sum of some amplitude-attenuated, time-delayed, and Doppler-scaled versions of the source signal (Li and Preisig, 2007). The traditional method for estimating the delay-Doppler parameters is matched filtering (MF), which estimates the cross-ambiguity function (CAF) between the received signal and the source signal (Jiang et al., 2011; Zeng and Xu, 2012). Yu and Yang estimated the delay-Doppler of target echo using the CAF method and the fractional Fourier transform method to restore the performance of matched filtering (Yu et al., 2017). Josso and Ioana proposed the Doppler compensation techniques based on CAF, which was accomplished by selecting a column corresponding to the absolute maximum in the ambiguity plane (Jossoet al., 2009). However, each multipath ray has a different Doppler scale dependent on its angle of emission. In consequence, the motion effect compensation with constant speed brings errors in estimating the delay-Doppler parameters.

The shallow water propagation channel can be characterized by sparsity (Wu et al., 2020), and the estimation of the channel impulse response (CIR) based on sparse representation has been a hot topic for decades of years (Cotter and Rao, 2002; Li et al., 2019; Wu et al., 2018). The CIR is directly connected with the delay-Doppler parameters of the multipath propagation. Considering that the resolution of the matched filtering is limited to the time-bandwidth product, the researchers investigated a sparse representation based method to improve the resolution of delay-Doppler estimation. Sparse representation methods based on basis pursuit (BP) criterion perform well with high accuracy and resolution, but they are inefficient with a very large dictionary matrix (Chen et al., 2001). The orthogonal matching pursuit (OMP) is one of the greedy pursuit algorithms and it is faster than standard approaches based on BP in most cases (Troppand Gilbert, 2007). Actually,

* Corresponding author. School of Marine Science and Technology, Northwestern Polytechnical University, Xi'an, 710072, China.
E-mail address: wfy@nwpu.edu.cn (F.-Y. Wu).

https://doi.org/10.1016/j.oceaneng.2021.109125
Received 24 November 2020; Received in revised form 19 March 2021; Accepted 3 May 2021
Available online 25 May 2021

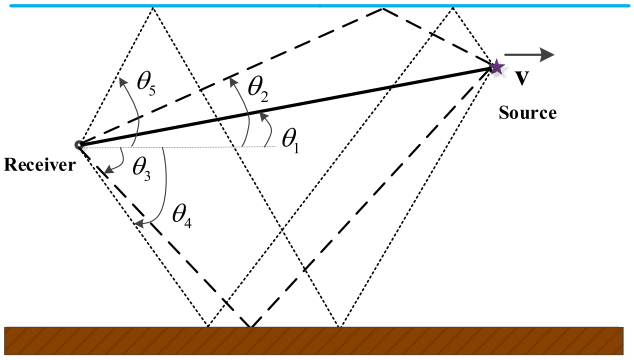

Fig. 1. The multipath propagation model of the ideal waveguide in shallow water.

$$d_k = \frac{c}{c - v_k} \approx 1 + \frac{v_k}{c}, \tag{2}$$

only the headmost several multipath arrivals need to be distinguished, which can be implemented by setting the sparse level K in the iterative process. By conducting an experiment, this paper investigates the effects of a moving source on the time delay and Doppler scale of multipath propagations in shallow water using the LFM signals. Without loss of generality, it is assumed that the source and receiver are in the same vertical plane and only the headmost five paths are analyzed here. The headmost five paths in shallow water are the direct (D) wave, the surface-reflected (SR) wave, the bottom-reflected (BR) wave, the surface-reflected-bottom-reflected (SB) wave, and the bottom-reflected-surface-reflected (BS) wave. The formulations of the Doppler scales of five paths resulted from a moving source are presented in this paper.

The delay-Doppler parameters corresponding to the five paths can be estimated by using sparse representation, which improves the resolution and accuracy. Considering the large scale of the dictionary matrix, we adopt the greedy algorithm to estimate the delay-Doppler parameters (Tropp, 2004). Different from the standard OMP method that requires matrix inversion, which leads to a huge consumption of computing resources and limits the applications for OMP, a modified greedy pursuit algorithm called Gram-Schmidt orthonormal matching pursuit (GSOMP) is proposed in this paper. We design an orthonormal basis at each iteration and thus avoids the computing of the inverse matrix to improve the robustness of the algorithm. The conventional CAF and non-greedy LS methods are compared with the proposed method. In addition, other greedy algorithms including regularized orthogonal matching pursuit (ROMP) (Needell and Vershynin, 2010) and Compressive Sampling MP (CoSaMP) (Needell and Tropp, 2009) are also compared with the proposed GSOMP method. Simulation results show that the proposed GSOMP algorithm is well performed in estimating the delay-Doppler parameters, which has advantages of high resolution and accuracy. The superiority of the proposed algorithm is further confirmed by at-sea experiments.

2. The sparse representation model

The model of a source with uniform linear motion in the isovelocity waveguide is presented in Fig. 1. The headmost five paths are investigated since they contain relatively large energy. The signals propagating through the five paths arrive at the receiver with different grazing angles, which are denoted as θ_k, $k = 1, 2, \ldots, 5$. Assuming the sea surface and sea bottom are flat, the motion vector $\vec{v}$ is then projected on the path of the kth ray with the grazing angle θ_k, which leads to

$$v_k = \|\vec{v}\|\cos(\theta_k), \tag{1}$$

where v_k is the radial velocity of the source relative to the receiver of the kth ray. Note that v_k is defined as positive when the source is approaching the receiver and negative when they are moving far away from each other. The Doppler scale corresponding to the kth path can be written as.where c is the sound speed. The Doppler scale d_k is dependent on the ratio of the radial velocity v_k to the sound speed c. The five paths have different propagation lengths resulting in different arrival times at the receiver. Let τ_k denotes the time delay of the kth path and consider the attenuation coefficient a_k of each ray, then the signal received at the time t for the$k$thray is expressed as

$$r_k(t) = a_k x(d_k(t - \tau_k)), \tag{3}$$

where $x(t)$ is the source signal. The received signal$r(t)$ is the sum of all the $r_k(t)$ arriving at the receiver, which leads to the following expression

$$r(t) = \sum_{k=1}^{K} a_k x(d_k(t - \tau_k)) + w(t), \tag{4}$$

where $w(t)$ is the additive Gaussian noise, and K is the number of multipath.

In Eq. (4), we find the received signal $r(t)$ can be represented as a sum of K signals parameterized by the undetermined parameters of $\{a_k, d_k, \tau_k\}$. Let Δt, $\Delta d$and $\Delta\tau$ denote the interval of the observing time, Doppler scale, and time delay, respectively. The discrete observing time is

$$t_n = n\Delta t,\ n = 0, \cdots, N-1, \tag{5}$$

where N is the length of the received signal. The discrete parameter sets of (d, τ) are defined as

$$d \in \mathbf{S}_d = \{d_0, d_0 + \Delta d, \cdots, d_0 + (L-1)\Delta d\}, \tag{6}$$

$$\tau \in \mathbf{S}_\tau = \{\tau_0, \tau_0 + \Delta\tau, \cdots, \tau_0 + (M-1)\Delta\tau\}, \tag{7}$$

where d_0 and τ_0 are the minimum possible Doppler scale and minimum possible time delay, respectively. There are L and M candidate values for d and τ, which means that LM possible columns need to be established. Let $\Delta t = \Delta\tau = 1/f_s$ and f_s is the sampling frequency of the received signal. Thus the sparse representation form of $r(t)$ can be written as

$$\boldsymbol{r} = \mathbf{X}\boldsymbol{h} + \boldsymbol{w}, \tag{8}$$

where $\boldsymbol{r} = [r(n\Delta\tau)]^T, \boldsymbol{w} = [w(n\Delta\tau)]^T, n = 0, \ldots, N-1$, which are the discrete received signal vector and noise vector, respectively. The matrix $\mathbf{X}$ is the so-called redundant dictionary, which has the following block form

$$\mathbf{X} = [\mathbf{X}_1, \ldots, \mathbf{X}_L], \tag{9}$$

$$\mathbf{X}_i = \begin{bmatrix} x(d_i 0) & 0 & \cdots & 0 \\ x(d_i\Delta_\tau) & x(d_i 0) & \cdots & \vdots \\ \vdots & \vdots & \ddots & \vdots \\ x(d_i(N-1)\Delta_\tau) & x(d_i(N-2)\Delta_\tau) & \cdots & x(d_i(N-M)\Delta_\tau) \end{bmatrix}, \tag{10}$$

where each block $\mathbf{X}_i (i = 1, \cdots, L)$ is the $N \times M$Toeplitz matrix corresponding to the ith searched Doppler scale parameter in the searching space of $\mathbf{S}_d$.

The unknown vector $\boldsymbol{h}$ in Eq. (8) is to be determined and it can be written as

$$\boldsymbol{h} = [\boldsymbol{h}_1, \ldots, \boldsymbol{h}_L]^T, \tag{11}$$

where

$$\boldsymbol{h}_j = \left[h_j(1), \ldots, h_j(M)\right]^T, j = 1, \ldots, L. \tag{12}$$

The delay-Doppler parameters can be estimated by solving Eq. (8).

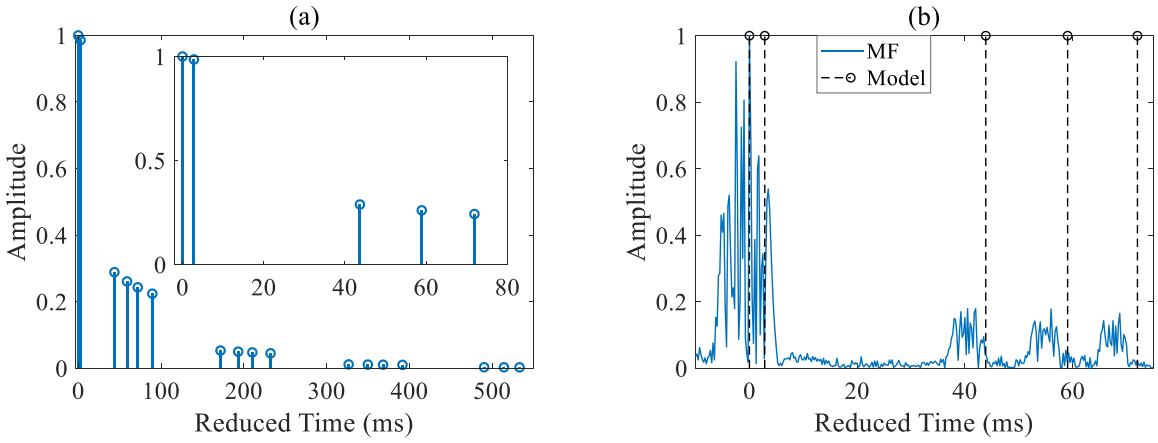

Fig. 2. The simulated results of (a) the CIR; (b) the direct MF result. The modeled time delays produced by Bellhop are marked by the dashed line that point out the referenced locations.

There are LM combinations of the delay-Doppler parameter as candidates, and the length of $\boldsymbol{h}$ is LM, thus the nonzero elements in $\boldsymbol{h}$ correspond to different delay-Doppler parameters. Therefore, we can reshape the variable $\boldsymbol{h}$ to a $L \times M$ matrix and then obtain the estimated results of super resolution in the delay-Doppler domain.

The traditional way to obtain the estimation of $\boldsymbol{h}$ is based on the LS criterion and the objective function can be expressed as (Vaccaro et al., 1992)

$$\boldsymbol{h}_{LS} = \underset{\boldsymbol{h}}{\arg\min} \|\boldsymbol{r} - \mathbf{X}\boldsymbol{h}\|^2 \tag{13}$$

Actually, the matrix $\mathbf{X}$ is an over-complete matrix if $N < LM$. The solution of the LS method can be obtained as

$$\boldsymbol{h}_{LS} = \left(\mathbf{X}^T\mathbf{X}\right)^{-1}\mathbf{X}^T\boldsymbol{r}. \tag{14}$$

The estimation result is not accurate enough since the LS method has no any constraints on the equation.

The received signal $\boldsymbol{r}$ is the linear combinations of the K columns in the dictionary matrix $\mathbf{X}$. The number of paths K is generally much smaller than LM, which means the solution of Eq. (8) is sparse. Then Eq. (8) can be adapted as an optimization problem

$$\min_{\boldsymbol{h}} \|\boldsymbol{h}\|_0 \ \text{ s.t. } \ \boldsymbol{r} = \mathbf{X}\boldsymbol{h}, \tag{15}$$

where $\|\|_0$ denotes the l_0-norm which is defined as the number of nonzero elements in the vector.

One useful method to solve Eq. (15) is compressed sensing (CS), which can be empirically divided into two groups: the greedy pursuit algorithms (e.g., OMP) and convex optimization algorithms such as basis pursuit de-noising (BPDN) (Figueiredoet al., 2007). The dimension of the matrix $\mathbf{X}$ is $N \times LM$ and it could be very large in practical applications. The computational complexity of the OMP and BPDN methods are $O(NLMK)$ and $O(N^2(LM)^3)$, respectively (Choi et al., 2017). Consequently, the computational cost of BPDN is larger than that of OMP. However, the OMP method has to calculate inverse matrix in the iterative process. A greedy pursuit algorithm called GSOMP is specifically designed to avoid the inverse matrix and improve the robustness. The GSOMP creates an orthonormal basis at each iteration to make the support space consisted of orthonormal bases. The details of the GSOMP algorithm are as follows.

Gram-Schmidt orthonormal matching pursuit algorithm

Input: Measurement vector $\boldsymbol{r}$, redundant dictionary $\mathbf{X}$, sparse level K
Initialization: Let the residual $\boldsymbol{e}_0 = \boldsymbol{r}$, index set $\Lambda_0 = \varnothing$, support space $\mathbf{X}_0 = \varnothing$, iteration index $i = 1, \widehat{\boldsymbol{h}} = \text{zeros}(LM, 1)$;
Step 1: Find $\lambda_i = \arg\max_{j=1,\cdots,ML} |\langle \boldsymbol{e}_{i-1}, \boldsymbol{x}_j \rangle|$, where $\boldsymbol{x}_j$ denotes the jth column of the matrix $\mathbf{X}$, $\langle \boldsymbol{e}_{i-1}, \boldsymbol{x}_j \rangle$is the inner product of $\boldsymbol{e}_{i-1}$ and$\boldsymbol{x}_j$, λ_i is the selected index;
Step 2: Update the index set and support space, $\Lambda_i = \Lambda_i \cup \{\lambda_i\}$, $\mathbf{X}_i = \mathbf{X}_{i-1} \cup \boldsymbol{x}_\lambda$, where $\boldsymbol{x}_\lambda$ denotes the λ_ith column of $\mathbf{X}$;
Step 3: Establish the Gram-Schmidt orthonormal basis of $\mathbf{X}_i$, denoted as $\mathbf{B}_i$ and each column of $\mathbf{B}_i$ is unitized to keep a unit length;
Step 4: Calculate $\widehat{\boldsymbol{h}}_i = (\mathbf{B}_i{}^T\mathbf{B}_i)^{-1}\mathbf{B}_i{}^T\boldsymbol{r}$ by the least square criterion, noting that $\mathbf{B}_i{}^T\mathbf{B}_i = \boldsymbol{I}$ and $\boldsymbol{I}$ is the identity matrix, then $\widehat{\boldsymbol{h}}_i = \mathbf{B}_i{}^T\boldsymbol{r}$, the matrix inversion operation is removed;
Step 5: Update $\boldsymbol{e}_i = \boldsymbol{r} - \mathbf{B}_i\widehat{\boldsymbol{h}}_i$;
Step 6: $i = i + 1$; if $i \le K$ go back to Step 1, otherwise stop the iteration.
Output: $\widehat{\boldsymbol{h}}(\Lambda) = \mathbf{B}^T\boldsymbol{r}$

The support space is denoted as $\mathbf{X}_i = [\boldsymbol{x}_1, \boldsymbol{x}_2, \ldots, \boldsymbol{x}_i]$, where $\boldsymbol{x}_i$ is the selected column vector in each iteration and the length of $\boldsymbol{x}_i$ is N. Let $\mathbf{B}_i = [\boldsymbol{b}_1, \boldsymbol{b}_2, \ldots, \boldsymbol{b}_i]$ represent the orthonormal basis of the space $\mathbf{X}_i$. Based on the Gram-Schmidt method, we have

$$\begin{aligned}
&\boldsymbol{e}_1 = \boldsymbol{x}_1, \boldsymbol{b}_1 = \frac{\boldsymbol{e}_1}{\|\boldsymbol{e}_1\|},\\
&\ldots\\
&\boldsymbol{e}_i = \boldsymbol{x}_i - \langle \boldsymbol{x}_i, \boldsymbol{b}_1 \rangle \boldsymbol{b}_1 - \langle \boldsymbol{x}_i, \boldsymbol{b}_2 \rangle \boldsymbol{b}_2 - \cdots - \langle \boldsymbol{x}_i, \boldsymbol{b}_{i-1} \rangle \boldsymbol{b}_{i-1},\\
&\boldsymbol{b}_i = \frac{\boldsymbol{e}_i}{\|\boldsymbol{e}_i\|};
\end{aligned} \tag{16}$$

where $\langle\rangle$ denotes inner product.

Noting that the size of the support space is $N \times i$ at the i-th iteration. The computational complexity of the matrix inversion in the OMP method is $O(i^3 + Ni^2)$, while the computational complexity of the Gram-Schmidt operation in the GSOMP method is $O(N + Ni^2)$. In general case, the dominant computational complexity in both operation is $O(Ni^2)$. The computational cost of the GSOMP method is similar to that of the OMP method so that the GSOMP method maintains the computational efficiency. Moreover, the proposed GSOMP method avoids the matrix

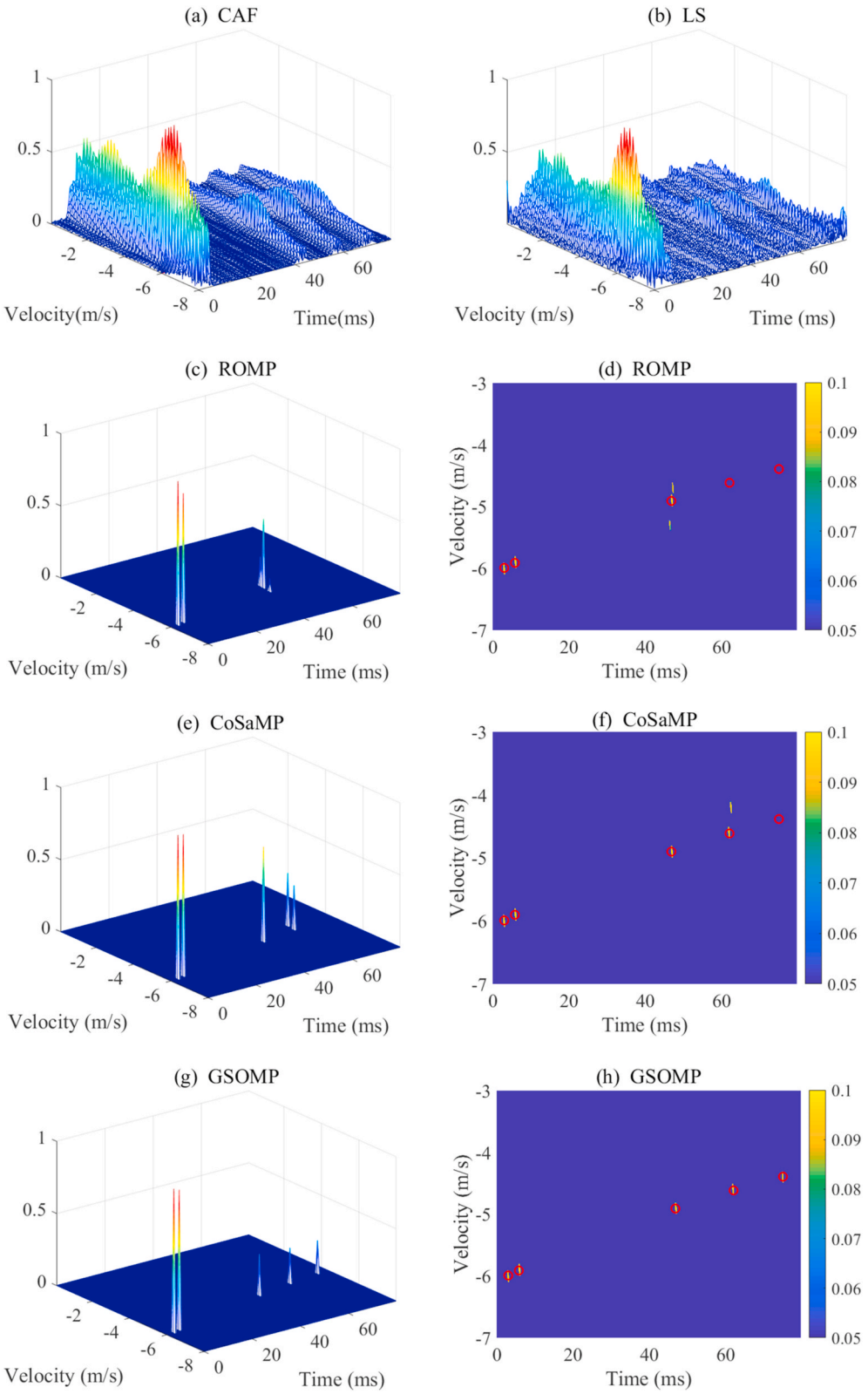

Fig. 3. The delay-Doppler estimation results with different methods: surface plots of (a) by the CAF, (b) by the LS; plots of (c, d) by the ROMP, (e, f) by the CoSaMP, (g, h) by the proposed GSOMP. The ambiguity plane in (d, f, h) present the comparisons between the estimated values and the referenced values represented by the red circle. (For interpretation of the references to colour in this figure legend, the reader is referred to the Web version of this article.)

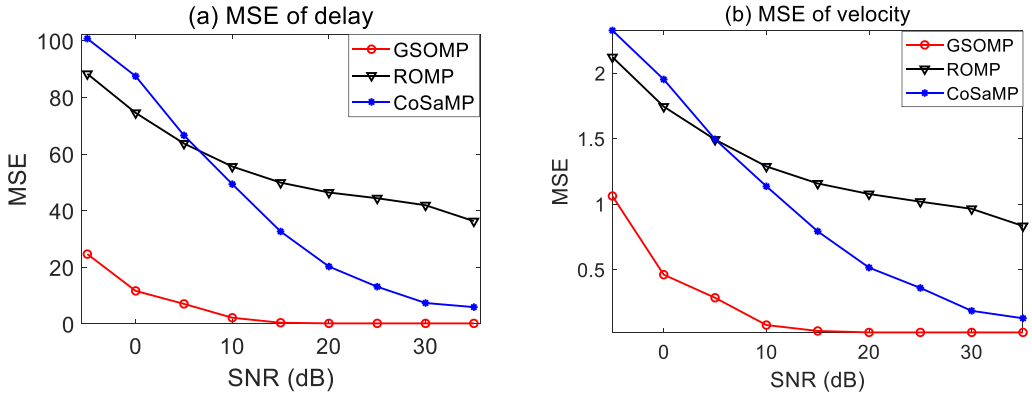

Fig. 4. The mean square error of (a) the estimated time delay versus SNR and (b) the estimated radial velocity versus SNR.

inversion thus to improve the robustness. It should be noticed that the output result contains information about the estimated Delay-Doppler parameters.

3. Simulation results

The LFM signal emitted by the source with starting frequency f_0 and pulse duration T can be expressed as

$$x(t) = \begin{cases} \cos\left(2\pi\left(f_0 t + \frac{k}{2}t^2\right)\right), & \text{if} 0 \le t \le T \\ 0 & \text{otherwise,} \end{cases} \tag{17}$$

where k is the chirp rate and the bandwidth of $x(t)$ can be derived as $W = kT$. The simulated LFM signal has a starting frequency of 2000 Hz, a bandwidth of 2000 Hz, a sampling frequency of 8000 Hz, and a pulse duration of 1 s. In the simulation, the receiver is fixed at a depth of 35 m; the source is moving at a constant velocity of 6 ms^{-1} at a depth of 20 m and 300 m away from the receiver on a 134 m deep channel, which has a constant sound speed of 1530 ms^{-1}. The simulated received signal is generated by convolving the source signal with the modeled CIR, which is produced by the acoustic ray model named Bellhop (Porter and Bucker, 1987). Furthermore, the Gaussian white noise with the signal-to-noise ratio (SNR) of 15 dB is added to the received signal. Considering the source is moving away from the receiver, the received signal will be stretched thus the observing time window is set as 1.5 s. The modeled CIR is shown in Fig. 2 (a), where the sparsity of the channel is illustrated. The direct MF result of the received signal is shown in Fig. 2 (b), which indicates that the time delays cannot be estimated with strong Doppler effects by the conventional MF method.

3.1. Comparison of different methods

The relative radial velocity is utilized to represent the corresponding Doppler scale based on Eq. (2) to show the estimated results more intuitively. The search space of the radial velocity is from −8 to 0 ms^{-1} with the precision of 0.1 ms^{-1}. Hence the dimension of the Doppler scale is $L = 80$. The search space of the time delay is from 0 to 80 ms with the precision $\Delta\tau = 1/f_s = 0.125$ ms, which leads to the dimension of the time delay $M = 640$. The observing length of the received signal vector is 8000, and consequently, there are $N = 8000$ rows and $LM = 51{,}200$ columns in the matrix $\mathbf{X}$. The sparse level used in the simulation is $K = 5$ because only the headmost five paths in the received signals are considered.

The time-delay and radial velocity estimations via different methods are shown in Fig. 3, where five paths can be found in the surface plots by the CAF and LS methods. The LS method has a similar performance with the CAF method as demonstrated in Fig. 3(a) and (b). For the CAF and LS methods, only the global maximum point can be determined while other local maximum points corresponding to the latter arrivals cannot be identified easily. In fact, each path has a different apparent speed and time delay for multipath propagations in shallow water. The GSOMP method outperforms the traditional CAF and LS methods in terms of resolution, which is demonstrated in Fig. 3(g). The GSOMP method enables the five paths to be distinguished in the surface plot, thus the corresponding delay and radial velocity of each path can be found easily. The estimated results of the ROMP and CoSaMP methods are shown in Fig. 3(c and d) and Fig. 3(e and f), respectively, which cannot provide accurate time delay of the channel compared with the GSOMP method.

The estimated results by the proposed GSOMP method are consistent with the referenced values shown in Fig. 3 (h), which indicates the high accuracy of the proposed GSOMP method. The red circle and the

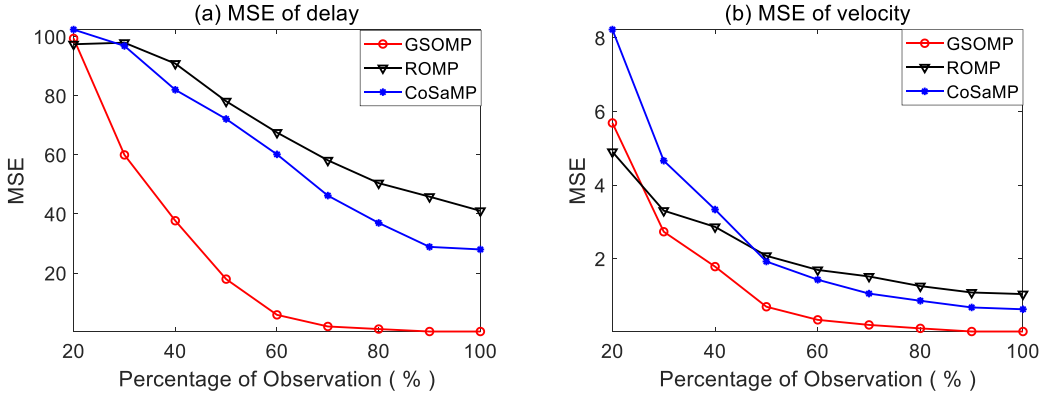

Fig. 5. The mean square error of (a) the estimated time delay versus percentage of observation and (b) the estimated radial velocity versus percentage of observation.

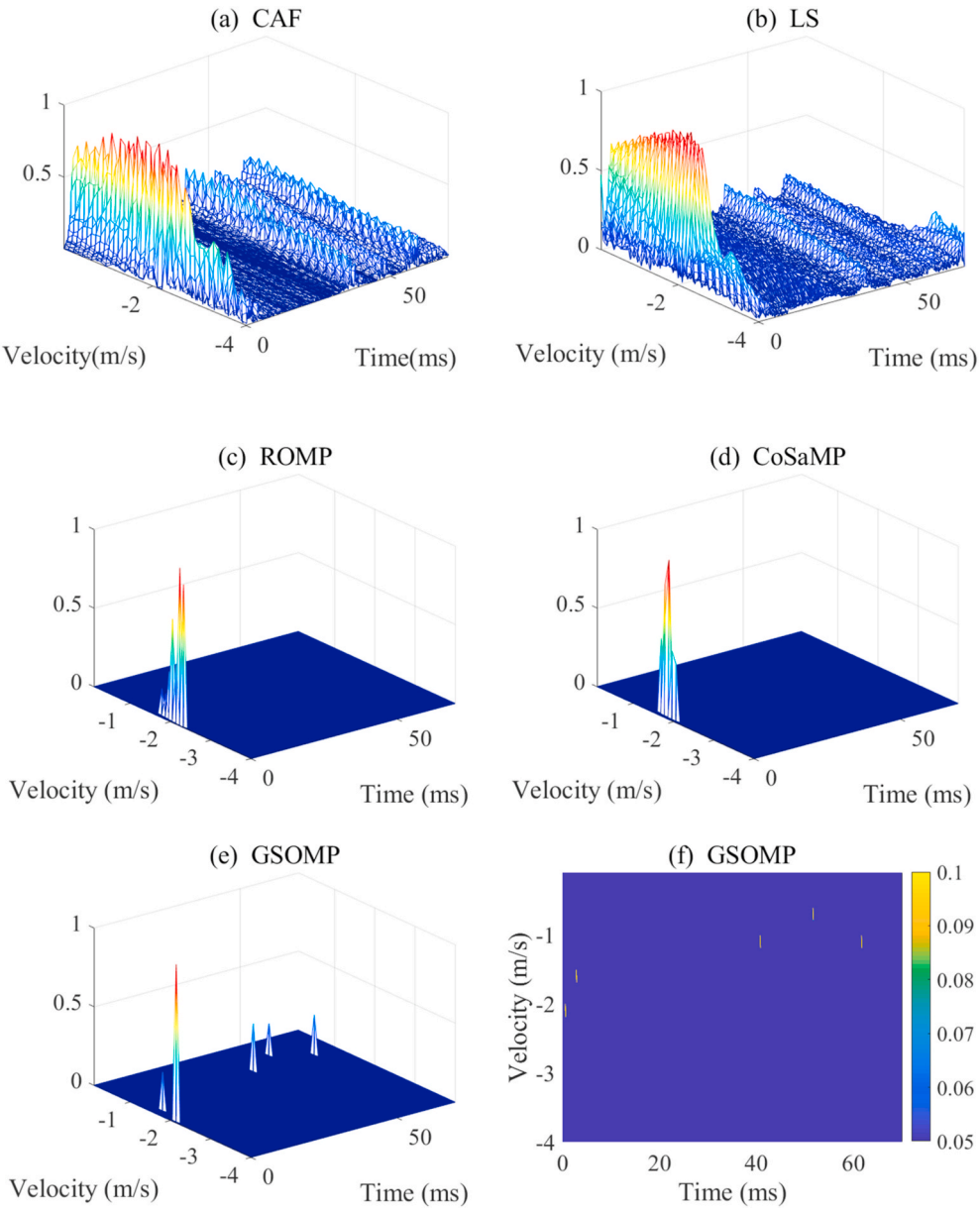

Fig. 6. The delay-Doppler estimation results of the real data: surface plots of (a) by the CAF, (b) by the LS, (c) by the ROMP, (d) by the CoSaMP, and (e) by the GSOMP method; (f) the ambiguity plane of the estimated results by the GSOMP method.

highlighted strip in Fig. 3 (h) denote the referenced and the estimated results, respectively. The estimated radial velocity of the first path is almost -6 ms^{-1} while that of the last path is about -4.4 ms^{-1} which means each path has a different radial velocity resulted from the different grazing angle. One can see that the exact time delay information is estimated by the proposed method instead of the ROMP and CoSaMP methods.

3.2. Statistical performance analysis

The statistical performances of the proposed GSOMP compared with the ROMP and CoSaMP methods are presented in this section. Because of the low resolution of the CAF and LS methods, it's difficult to extract the delay-Doppler parameters in the ambiguity plane. Therefore we do not compare the CAF and LS methods in this subsection. The mean square error (MSE) of the estimated time delay and radial velocity can be respectively expressed as

$$\mathrm{MSE}_{\tau} = \frac{1}{M_C}\sum_{n=1}^{M_C} \|\hat{\boldsymbol{\tau}} - \boldsymbol{\tau}\|^2 \tag{18}$$

and

$$\mathrm{MSE}_{V} = \frac{1}{M_C}\sum_{n=1}^{M_C} \|\hat{\mathbf{v}} - \mathbf{v}\|^2, \tag{19}$$

where M_C is the number of independent trials; $\hat{\boldsymbol{\tau}}$ and $\hat{\mathbf{v}}$ are the estimated time delay and radial velocity, respectively.

The CIR is the same as that in the subsection 3.1. The SNR and the measurement length are the two main parameters that affect the performance of the methods. Noting the measurement length is denoted by the percentage of observation, which means different percentages of the received signal are selected from the starting time of the signal. The number of independent trials is set as $M_C = 200$ during the simulation. The SNR of the received signal varies from -5 dB to 35 dB with a step of

Table 1
The estimated delay results by the GSOMP method compared with the modeled delay results.

Path	Estimated delay (ms)	Modeled delay (ms)
D	0	0
SR	2.25	1.71
BR	40.13	39.89
SB	51.00	51.01
BS	61.00	61.91

5 dB. The percentage of observation represents the length of measurements and varies from 20% to 100% with a step of 10%.

The MSEs of the estimated time delay and radial velocity versus SNR are displayed in Fig. 4, where we find the GSOMP method can estimate the delay-Doppler parameters with high accuracy when the SNR is larger than 15 dB. Similarly, the MSEs versus percentage of observation are shown in Fig. 5, where the proposed GSOMP method yields quite low MSEs when the percentage of observation is larger than 60%. When the percentage of length reaches 80%, the MSE_τ and the MSE_V of the GSOMP method are 1.047 and 0.106, respectively.

4. Experimental results

The shallow water acoustic experiment was conducted in the East China Sea in January 2015. The experimental area was nearly flat and the water depth was about 134 m. The sound speed profile (SSP) collected during the experiment shows a typical characteristic of the mixed layer in winter, which has a mean speed of 1530 ms^{-1}. The hydrophone was anchored at the depth of 30.8 m and the source emitting LFM signals was towed by the vessel with linear motion at a speed of 2.5 ms^{-1}. The LFM has a starting frequency of 2000 Hz, a bandwidth of 2000 Hz, and a duration of 1 s. A depth sensor was tied to the moving source, which indicates the source depth is 16.6 m. The horizontal distance between the source and the receiver is 364.5 m, which is derived from the global positioning system (GPS). It is coincident that the moving direction of the source is almost consistent with the attachment direction between the source and the receiver. The sampling rate of the hydrophone is $f_s = 8000$ Hz. The SNR of the received signal is about 22 dB within the narrow frequency band of the source signal.

The minimum, maximum, and the search interval of the radial velocity are set as $v_{\min} = -4$ ms^{-1}, $v_{\max} = 0$ ms^{-1}, and $\Delta v = 0.1$ ms^{-1}, respectively. Then the Doppler scale can be obtained from Eq. (2). Noting that the Doppler effect resulted from a number of factors in real applications and the radial velocity used here is the result of the conversion. The search space of the time delay is set $\tau_{\min} = 0$, $\tau_{\max} = 70$ ms, and $\Delta\tau = 1/f_s = 0.125$ ms. The observing length of the received signal vector is 8000, thus there are $N = 8000$ rows and $LM = 22{,}400$ columns in the dictionary matrix $\mathbf{X}$.

The surface plots of the CAF and LS methods with real data are shown in Fig. 6 (a) and (b), respectively, which reveal five apparent paths in the first 70 ms. But the resolution of the CAF and LS methods is limited that they cannot determine the specific parameters of each path. The sparse level is set $K = 5$ and estimations of the GSOMP method are shown in Fig. 6 (e) and (f), respectively. The estimated parameters can be determined via the proposed GSOMP method simply and directly. The results demonstrate the high resolution of the GSOMP method in estimating the delay-Doppler parameters. As comparisons, the surface plots of the ROMP and CoSaMP methods are shown in Fig. 6 (c) and (d), respectively. The ROMP and CoSaMP methods fail to separate the multipath arrivals due to the existing environment noise and these two methods selected multiple column vectors in each iteration so that more interference were introduced in the process.

The estimated radial velocity by the GSOMP method of the first path is -2.1 ms^{-1}, which is close to the real moving speed (-2.5 ms^{-1}) of the source. The radial velocity is a converted result of the total Doppler effects, therefore, the difference exists between the estimated results and the modeled values. From Fig. 6 (f), it is clear that each path has different delay-Doppler parameters. The comparisons between the estimated time delays by the GSOMP method and the modeled delays are shown in Table 1, where the modeled values of the multipath arrivals are Bellhop-predicted. The estimated time delays by the GSOMP method are close to the model-predicted delays. Thus it is reasonable that the accuracy of our method is verified.

5. Conclusions

In view of the shortcomings of the CAF method on estimating delay-Doppler parameters, a sparse representation-based method for moving LFM signals is proposed in this paper to improve the resolution and accuracy of the estimation results. Since the dictionary matrix is often large in practical problems, the improved GSOMP method is used to solve the sparse representation model, which can avoid the calculation of inverse matrices in the iterative process and improve the robustness of the algorithm to facilitate its application. The CAF, LS, ROMP and CoSaMP methods are compared with the proposed method in simulations and experiments. The results indicate the proposed method performs well in estimating the multipath delay-Doppler parameters both in terms of resolution and accuracy. Furthermore, the proposed method may be applied to radial velocity measurement, active sonar target detection and passive acoustic tomography in the future.

Declaration of competing interest

The authors declare that they have no known competing financial interests or personal relationships that could have appeared to influence the work reported in this paper.

Acknowledgement

The authors would like to thank all of the experiment participants on the vessel for their hard work to make this experiment successful. This work is supported by the National Natural Science Foundation of China under Grant No. 61701405, the Fundamental Research Funds for the Central University under Grant No. 3102019HHZY030011.

References

Cao, X.-l., Jiang, W.-h., Tong, F., 2018. Time reversal MFSK acoustic communication in underwater channel with large multipath spread. Ocean. Eng. 152, 203–209.
Chen, S.S., Donoho, D.L., Saunders, M.A., 2001. Atomic decomposition by basis pursuit. SIAM Rev. 43 (1), 129–159.
Choi, J.W., Shim, B., Ding, Y., Rao, B., Kim, D.I., 2017. Compressed sensing for wireless communications: useful tips and tricks. IEEE Commun. Surv. Tut. 19 (3), 1527–1550.
Cotter, S.F., Rao, B.D., 2002. Sparse channel estimation via matching pursuit with application to equalization. IEEE Trans. Commun. 50 (3), 374–377.
Figueiredo, M.A., Nowak, R.D., Wright, S.J., 2007. Gradient projection for sparse reconstruction: application to compressed sensing and other inverse problems. IEEE J. Sel. Top. Signal Process. 1 (4), 586–597.
Jesus, S.M., Porter, M.B., Stéphan, Y., Démoulin, X., Rodríguez, O.C., Coelho, E.M.F., 2000. Single hydrophone source localization. IEEE J. Ocean. Eng. 25 (3), 337–346.
Jiang, X., Zeng, W.J., Li, X.L., 2011. Time delay and Doppler estimation for wideband acoustic signals in multipath environments. J. Acoust. Soc. Am. 130 (2), 850–857.
Josso, N.F., Ioana, C., Mars, J.I., Gervaise, C., Stéphan, Y., 2009. On the consideration of motion effects in the computation of impulse response for underwater acoustics inversion. J. Acoust. Soc. Am. 126 (4), 1739–1751.
Li, B., Zheng, S., Tong, F., 2019. Bit-error rate based Doppler estimation for shallow water acoustic OFDM communication. Ocean. Eng. 182, 203–210.
Li, W., Preisig, J.C., 2007. Estimation of rapidly time-varying sparse channels. IEEE J. Ocean. Eng. 32 (4), 927–939.
Liang, N., Yang, Y., Guo, X., 2019. Doppler chirplet transform for the velocity estimation of a fast moving acoustic source of discrete tones. J. Acoust. Soc. Am. 145 (1), EL34–EL38.
Mandic, F., Miskovic, N., Loncar, I., 2020. Underwater acoustic source seeking using time-difference-of-arrival measurements. IEEE J. Ocean. Eng. 45 (3), 759–771.
Needell, D., Tropp, J.A., 2009. CoSaMP: iterative signal recovery from incomplete and inaccurate samples. Appl. Comput. Harmon. Anal. 26 (3), 301–321.

Needell, D., Vershynin, R., 2010. Signal recovery from incomplete and inaccurate measurements via regularized orthogonal matching pursuit. IEEE J. Sel. Top. Signal Process. 4 (2), 310–316.
Porter, M.B., Bucker, H.P., 1987. Gaussian beam tracing for computing ocean acoustic fields. J. Acoust. Soc. Am. 82 (4), 1349–1359.
Song, H., Cho, C., Hodgkiss, W., Nam, S., Kim, S.-M., Kim, B.-N., 2018. Underwater sound channel in the northeastern East China Sea. Ocean. Eng. 147, 370–374.
Tropp, J.A., 2004. Greed is good: algorithmic results for sparse approximation. IEEE Trans. Inf. Theor. 50 (10), 2231–2242.
Tropp, J.A., Gilbert, A.C., 2007. Signal recovery from random measurements via orthogonal matching pursuit. IEEE Trans. Inf. Theor. 53 (12), 4655–4666.
Vaccaro, R., Ramalingam, C., Tufts, D., Field, R., 1992. Least-squares time-delay estimation for transient signals in a multipath environment. J. Acoust. Soc. Am. 92 (1), 210–218.
Wu, F.-Y., Yang, K., Sheng, X., Huang, F., 2020. A blocked MCC estimator for group sparse system identification. AEU - Int. J. Electron. C. 115, 153033–153038.
Wu, F.-Y., Yang, K., Tong, F., Tian, T., 2018. Compressed sensing of delay and Doppler spreading in underwater acoustic channels. IEEE Access 6, 36031–36038.
Yu, G., Yang, T., Piao, S., 2017. Estimating the delay-Doppler of target echo in a high clutter underwater environment using wideband linear chirp signals: evaluation of performance with experimental data. J. Acoust. Soc. Am. 142 (4), 2047–2057.
Zeng, W.J., Xu, W., 2012. Fast estimation of sparse doubly spread acoustic channels. J. Acoust. Soc. Am. 131 (1), 303–317.